

Broadband spectroscopy of polymer waveguide and its sensing applications in the THz region

LIU Jing^{1,2}, XIAO Ming-Fei³, SHEN Jing-Ling^{2,*}, ZHANG Bo², ZHANG Wei³, ZHANG Cun-Lin^{1,2}

(1. School of Optoelectronics, Beijing Institute of Technology, Beijing 100081, China;

2. Beijing Key Laboratory for Terahertz Spectroscopy and Imaging, Key Laboratory of Terahertz Optoelectronics, Ministry of Education, Department of Physics, Capital Normal University, Beijing, 100048, China;

3. Tsinghua National Laboratory for Information Science and Technology, State Key Laboratory on Integrated Optoelectronics, Department of Electronic Engineering, Tsinghua University, Beijing 100084, China)

Abstract: A broadband spectroscopy of anti-resonant waveguides in the terahertz region was investigated. The broadband spectral transmission properties of a poly(methylmethacrylate) (PMMA) pipe waveguide, a PMMA self-supporting waveguide, and a SiO₂ pipe waveguide were studied using terahertz time domain spectroscopy (THz-TDS). The existence of the anti-resonance phenomenon was demonstrated. Additionally, the PMMA self-supporting waveguide has been experimentally shown to realize transmission bandwidth of over 2 THz without dip frequencies. Also, based on the anti-resonance mechanism, the dielectric pipe waveguide was successfully used as a terahertz refractive index sensor for liquid sensing, which offers a possible method for materials detection.

Key words: polymer fiber optics, fiber optics sensors, terahertz spectroscopy, broadband transmission, anti-resonance

PACS: 84.40.-x, 42.81.Pa

太赫兹宽谱聚合物波导及其传感应用

刘婧^{1,2}, 肖鸣飞³, 沈京玲^{2,*}, 张波², 张巍³, 张存林^{1,2}

(1. 北京理工大学光电学院, 北京 100081;

2. 首都师范大学太赫兹光电子学教育部重点实验室, 北京 100048;

3. 清华大学电子工程系, 北京 100084)

摘要: 利用太赫兹时域光谱系统对三种反谐振波导的太赫兹谱进行了研究, 这三种波导分别是 PMMA 管型波导, PMMA 自支撑结构波导和 SiO₂ 管型波导. 该研究验证了三种波导的太赫兹传输基于反谐振理论, 并在实验上实现了 PMMA 自支撑结构波导超过 2 THz 的宽光谱传输. 同时, 对基于反谐振原理的太赫兹物质传感进行了理论和实验分析, 为物质探测提供了一种可行的手段.

关键词: 聚合物波导; 光纤传感器; 太赫兹光谱; 宽谱传输; 反谐振原理

中图分类号: TN814 文献标识码: A

Introduction

As terahertz (THz) technology develops rapidly in a variety of application areas, low propagation loss and flexible waveguides are regarded as an essential component for convenient THz communications^[1]. Therefore,

many different types of waveguides have been developed, including metallic waveguides^[2-4], micro-structured waveguides^[5-9], and Bragg waveguides^[10-12].

Compared with the metallic materials, dielectric waveguides can realize low loss and flexible bending. At the same time, broadband spectroscopy studies are highly important to the understanding of THz transmission prop-

Received date: 2016-01-07, **revised date:** 2016-07-08

收稿日期: 2016-01-07, **修回日期:** 2016-07-08

Foundation items: Supported by National Instrumentation Program (2012YQ140005); the Nature Science Foundation of Beijing (4144069); the Science and Technology Project of Beijing Municipal Education Commission (KM201410028004)

Biography: LIU Jing (1987-), female, PHD student, research area focus on terahertz waveguide spectroscopy etc. E-mail: newone_kaka@126.com

* **Corresponding author:** E-mail: sjl-phy@cnu.edu.cn

erties. Many types of waveguides based on various mechanisms have been investigated, and among them, the anti-resonant waveguide is considered the most effective way to transmit broadband THz waves^[13,14]. This waveguide is a thin pipe that consists of a large air core and a thin dielectric layer with uniform refractive index. Because of the anti-resonance mechanism, the power of the THz wave can be restricted within the air core, and only certain resonant modes can be leaked towards the exterior, which means that THz waves can be transmitted in the waveguide over a broad range of frequencies that are separated from the specific range where the so-called dip frequency is attained.

As to the dielectric material of such waveguides, both Cyclic olefin copolymer Topas (COC)^[15] and Polymethylmethacrylate (PMMA)^[14] have good optical transparency in terahertz band. Especially, PMMA have been widely used in polymer fibers thanks to its excellent characteristics for fiber fabrication. We have previously studied the properties of PMMA pipe waveguides^[16,17] and self-supported waveguides^[18] for THz continuous wave transmission. These waveguides can realize low loss propagation for THz waves at 3.1 THz. However, their broadband transmission properties have not been studied experimentally.

As part of our subsequent investigations, we present here the broadband transmission properties of these dielectric waveguides. Importantly, the self-supporting waveguide has been experimentally confirmed to have its designed broadband propagation properties. Also, it is already known that the dip frequency is related to the refractive indices of the cladding, which means that the dielectric pipe waveguide can be used as a THz refractive index sensor. In this paper, we also present our work on the liquid sensing applications of these polymer waveguides.

2 Propagation and sensing mechanism

A double-layer model can be used as the theoretical sensing model^[19]. The cross-sectional schematic of this model is shown in Fig. 1(a). During the THz transmission process, part of the THz wave is reflected at the interface between the two-layer structures, with a one-dimensional optical path as shown in Fig. 1(b).

When the light is grazing incidence into the waveguide, the resonance frequency can be derived as

$$f_m = \frac{mc}{2(d_1 \sqrt{n_1^2 - n_0^2} + d_2 \sqrt{n_2^2 - n_0^2})}, m = 1, 2, 3, \dots \quad (1)$$

where f_m is the resonant frequency, c is the velocity of light in a vacuum, m is an integer, n_0 is the refractive index of the environment, and d_1, d_2 and n_1, n_2 are the thicknesses and refractive indices of the double layer, respectively.

When $n_1 = n_0$, this formula can be simplified in the form of a one-layer model for the anti-resonant waveguide. The formula also shows that if n_0, n_2 and d_2 are known, then the refractive index n_1 or thickness d_1 of the waveguide can be determined when either of these parameters is tested. This suggests a new method of ma-

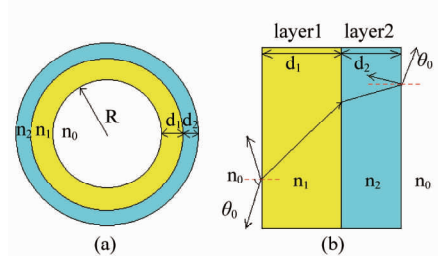


Fig. 1 (a) Cross-sectional schematic of the model, where n_0, n_1 , and n_2 are the refractive indices of the air, the sample layer and the cladding, respectively. R, d_1 , and d_2 are the radius of the inner pipe and the thicknesses of the different layers, respectively; (b) one-dimensional optical path of a THz wave reflected inside the waveguide

图 1 (a) 太赫兹反谐振波导双包层的横截面示意图, n_0, n_1, n_2 分别为空气、样品层和包层折射率, R, d_1, d_2 分别为空芯半径以及不同层的厚度, (b) 太赫兹波在波导层间传输的一维图示

terial sensing based on the anti-resonant waveguide.

Additionally, it is clear that the dip frequency is reduced when layer 1 exists, and this results in a red-shift of the frequency spectrum of the waveguide. Based on this mechanism, the dielectric pipe waveguide can successfully be used as a THz refractive index sensor for liquid sensing.

3 Broadband spectrum of the waveguide

The experimental setup for broadband THz waveguide and measurement of its sensing properties is shown in Fig. 2. It is a typical THz-TDS setup previously used to measure THz transmission spectra. In this case, the waveguide sample is placed at the THz beam waist in the parallel optical path between the parabolic mirrors PM3 and PM4 because a grazing incidence is required according to Eq. (1), as shown in Fig. 2. Two apertures are used to block off any stray light at the front and back of the waveguide. The spectrum of the system ranges from 0.2 THz to 2.6 THz. This system can be used to measure various waveguides with lengths up to 150 mm.

The PMMA pipe waveguide, the PMMA self-supporting waveguide and a SiO_2 pipe waveguide are used as the experimental samples. The theoretical refractive indices of PMMA and SiO_2 are 1.53 and 1.44, respectively. Cross-sectional schematics of the waveguides are shown in Fig. 3. The diameter of the PMMA pipe waveguide is 3.8 mm and the pipe cladding thickness is 0.2 mm, while the inner diameter of the SiO_2 pipe waveguide is 3 mm and its cladding thickness is 1 mm. The dimensions of the self-supporting waveguide are $r_h = 1$ mm, $R_h = 2$ mm, $t_h = 0.02$ mm, and $T_h = 0.2$ mm. All three pipes are 86 mm long.

Figure 4(a), (b) and (c) show the time-domain spectra for the PMMA pipe, the PMMA self-supporting pipe waveguide, and the SiO_2 pipe, respectively. The black curves of each graph are the responses of the waveguides to sample signals, while the red curves repre-

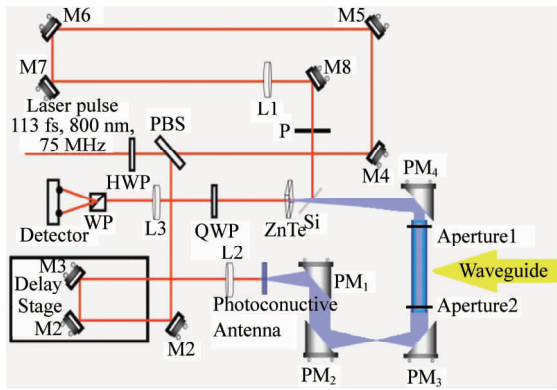


Fig. 2 Broadband THz waveguide experimental setup based on THz-TDS system

图 2 基于太赫兹时域光谱系统的宽谱太赫兹波导实验装置

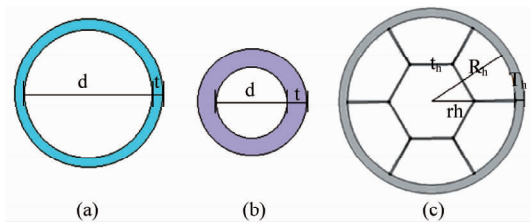


Fig. 3 Cross-sectional schematics of (a) the PMMA pipe, (b) the SiO_2 pipe and (c) the PMMA self-supporting waveguide

图 3 横截面示意图(a)PMMA 管型波导, (b) SiO_2 管型波导, (c)PMMA 自支撑结构波导

sent the responses to signals without these samples (i. e., reference signals). Because the group refractive indices^[6,20] of these terahertz waveguides are greater than the refractive index of air, all sample signals have temporal delays when compared with the reference signals. At the same time, the amplitudes of the sample signals are attenuated when compared with those of the reference signals because of material absorption losses and coupling losses.

Obvious spectrum dips at equal intervals can be observed in the transmission spectra of the three waveguides in the frequency domain, as indicated by the arrows in Fig. 5. The figure also shows that the measured spectral periodic frequencies of the PMMA pipe waveguide and the SiO_2 pipe waveguide are 0.32 THz and 0.18 THz, respectively, which are close to the corresponding periods of the resonance frequencies of 0.31 THz and 0.13 THz that were calculated using Eq. (1). The deviations in these values may be caused by cladding thickness variation and tiny differences between the actual and theoretical values of the refractive index. The cladding thickness of the waveguide is inversely proportional to the resonance frequency. Therefore, reduction of the wall thickness causes the resonance period to increase. The thickness of the self-supporting waveguide's inner wall is approximately 0.02 mm, and thus only one resonant peak can be observed in the range from 0.2 THz to 2.6 THz, which indicates that the waveguide can realize broadband THz propagation if the dimensions are designed properly. At resonant frequencies, transmission drops significantly

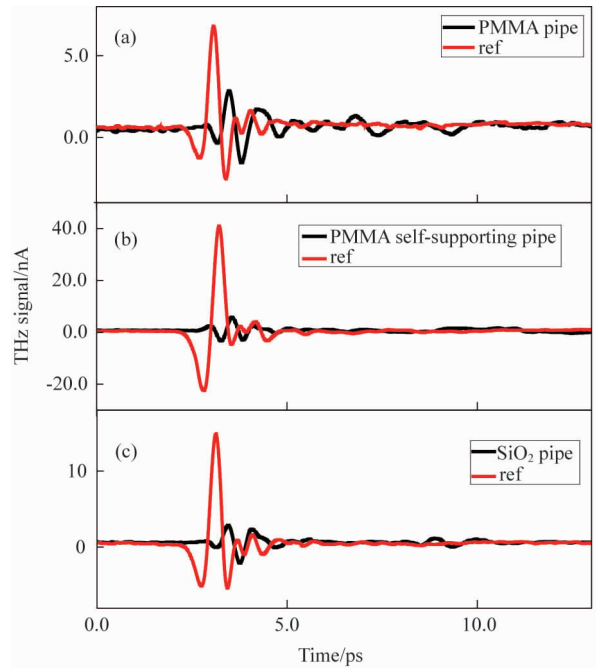


Fig. 4 THz time-domain spectra for (a) the PMMA pipe, (b) the PMMA self-supporting pipe, and (c) the SiO_2 pipe
图 4 (a) PMMA 管型波导, (b) PMMA 自支撑结构波导, (c) SiO_2 管型波导的太赫兹时域光谱图

because there are no core modes to deliver the THz power. It is clear that the transmission and resonance frequencies of these waveguides are well matched, and this indicates that the guiding mechanisms of the pipe waveguides are indeed anti-resonant reflective guiding mechanisms.

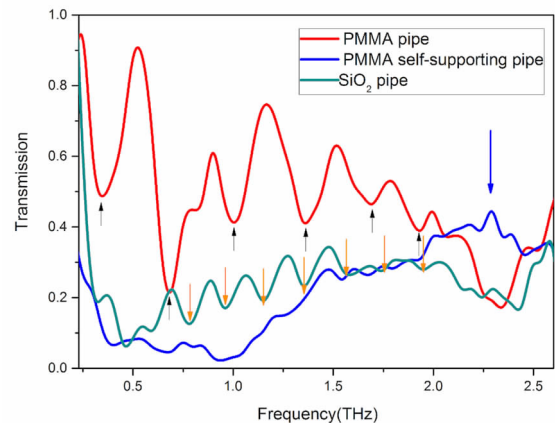


Fig. 5 Transmission spectra of the PMMA pipe waveguide, the PMMA self-supporting pipe and the SiO_2 pipe

图 5 (a) PMMA 管型波导, (b) PMMA 自支撑结构波导, (c) SiO_2 管型波导的太赫兹透射谱

4 Liquid sensing with the pipe waveguide

The waveguide used for the sensing experiment is the PMMA pipe waveguide. The pipe has a wall thickness of 0.2 mm, a diameter of 3.8 mm, and a length of 86 mm. The transmission properties of the pipe have

been studied above. Simulation and experimental results show that this type of pipe can transmit THz waves with low propagation losses over a wide frequency range. Soybean oil was chosen as the material to be detected. The refractive index of the oil was measured before the experiment by THz-TDS, and was found to be 1.27 in the 0.2 THz to 2.6 THz range.

During the experiment, soybean oil was dropped inside one of waveguide ends, and the inner wall of the waveguide was evenly covered with the soybean oil when the waveguide was tilted because of the effects of gravity and the surface tension of the oil droplets.

Figure 6 shows the transmission spectra of the polymer waveguide and waveguide with soybean oil. Obvious dip frequencies at equal intervals are observed, as indicated by the arrows in Fig. 6, and the interval is smaller than that of the waveguide without the oil coating. This therefore indicates that the measured spectral frequency dip shifts towards a lower frequency (redshift) when the pipe is coated with soybean oil. The redshift for each dip is uneven, which means that the redshift increases as the frequency increases, and the largest value that can be clearly observed in the frequency range of interest is approximately 40 GHz at around 1.5 THz, as shown in Fig. 6. The refractive index of PMMA is 1.53^[17], and the cladding thickness of the pipe is 0.2 mm, which means that if the refractive index or the thickness of the soybean oil coating is known, then the other variable can be calculated according to Eq. (1). Because the refractive index of the oil is measured as 1.27, the thickness of the soybean oil coating is then calculated to be about 0.34 mm. This value is approximately comparable with the actual thickness of the soybean oil when estimated based on the volume of oil divided by the inner surface area of the waveguide. This result shows that the pipe can be used as a liquid sensor in the THz region.

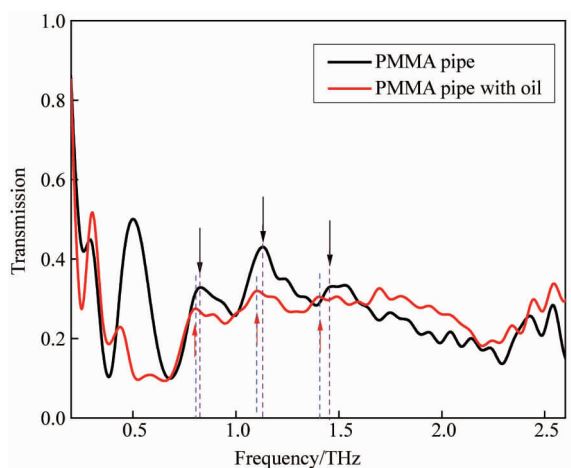


Fig. 6 Transmission spectra of the PMMA pipe waveguide with and without oil coating

图6 PMMA管型波导与其内壁均匀涂抹植物豆油后该波导的太赫兹透射谱

5 Conclusion

The results of our work on broadband spectroscopy

of anti-resonant waveguides in the THz region have been presented. Using a THz-TDS system, the broadband spectral transmission properties of a SiO₂ waveguide, a single-mode PMMA pipe waveguide and a PMMA self-supporting waveguide have been studied and spectrum dips have been observed at equal intervals, which demonstrated the existence of the anti-resonance phenomenon. The results also indicated that the PMMA self-supporting waveguide can realize broadband propagation of THz waves, with a measured bandwidth of more than 2 THz for a cladding thickness of 0.02 mm. Based on the anti-resonance mechanism, a PMMA pipe waveguide was successfully demonstrated as a THz refractive index sensor for liquid sensing. The sensing results match the actual values well, which means that these dielectric waveguides can provide a possible future method for liquid materials detection.

References

- [1] Atakaramians S, Afshar Vahid S, Monro T, et al. Terahertz dielectric waveguides[J]. *Advances in Optics & Photonics*, 2013, **5**(2):169–215.
- [2] Mendis R, Grischkowsky D. Undistorted guided-wave propagation of subpicosecond terahertz pulses. [J]. *Optics Letters*, 2001, **26**(11):846–8.
- [3] Zhan H, Mendis R, Mittleman D M. Characterization of the terahertz near-field output of parallel-plate waveguides[J]. *Journal of the Optical Society of America B*, 2011, **28**(3):558–566.
- [4] Gallot G, Jamison S P, McGowan R W, et al. Terahertz waveguides [J]. *Journal of the Optical Society of America B*, 2000, **17**(5):851–863.
- [5] Setti V, Vincetti L, Argyros A. Flexible tube lattice fibers for terahertz applications. [J]. *Optics Express*, 2013, **21**(3):3388–3399.
- [6] Bao H, Nielsen K, Rasmussen H K. Fabrication and characterization of porous-core honeycomb bandgap THz fibers. [J]. *Optics Express*, 2012, **20**(28):29507–17.
- [7] Lu J Y, Yu C P, Chang H C, et al. Terahertz air-core microstructure fiber[J]. *Applied Physics Letters*, 2008, **92**(6):064105–064105–3.
- [8] Andrews S R. Microstructured terahertz waveguides [J]. *Journal of Physics D Applied Physics*, 2014, **47**(37).
- [9] Bao H, Nielsen K, Rasmussen H K, et al. Design and optimization of mechanically down-doped terahertz fiber directional couplers. [J]. *Optics Express*, 2014, **22**(8):9486–9497.
- [10] Skorobogatiy M, Dupuis A. Ferroelectric all-polymer hollow Bragg fibers for terahertz guidance *Applied physics letters*, 2007, **90**(11):113514.
- [11] Yu R J, Zhang B, Zhang Y Q, et al. Proposal for Ultralow Loss Hollow-Core Plastic Bragg Fiber With Cobweb-Structured Cladding for Terahertz Waveguiding[J]. *IEEE Photonics Technology Letters*, 2007, **19**(12):910–912.
- [12] Wu Y, Yao B, Zhang A, et al. Graphene-coated microfiber Bragg grating for high-sensitivity gas sensing[J]. *Optics Letters*, 2014, **39**(5):1235–7.
- [13] Lai C H, You B, Lu J Y, et al. Modal characteristics of anti-resonant reflecting pipe waveguides for terahertz waveguiding. [J]. *Optics Express*, 2010, **18**(1):309–22.
- [14] Bao H, Nielsen K, Bang O, et al. Dielectric tube waveguides with absorptive cladding for broadband, low-dispersion and low loss THz guiding. [J]. *Scientific Reports*, 2015, **5**:7620–7620.
- [15] Nielsen K, Rasmussen H K. Bendable, low-loss Topas fibers for the terahertz frequency range. [J]. *Optics Express*, 2009, **17**(10):8592–601.

(下转第 533 页)

Table 1 Comparison of Ka-band amplifier MMIC**表 1 Ka 波段功放 MMIC 比较**

Ref.	process	Stages	Output matching	Freq/GHz	Gain/dB	PAE _{sat} /%	Pout _{sat} /dBm	Size/mm
[2]	0.15 μm pHEMT GaAs	1	Inductive	17 – 35	9 – 12	35 – 40	22.5 – 23.5	1.5 × 1
[5]	0.25 μm pHEMT GaAs	3	Inductive	31 – 37	15 – 18	27.5	23 – 25	2.43 × 1.28
[6]	0.15 μm pHEMT GaAs	3	Capacitive	30 – 38	22 – 25	20 – 36	35 – 36	3.6 × 2.75
[7]	0.15 μm pHEMT GaAs	3	NA	30 – 40	14 – 20	25	33 – 34	2.8 × 2.3
[8]	0.15 μm HEMT GaN	3	Inductive	26 – 33	24 – 31	28 – 35	37 – 38	3.24 × 1.74
[9]	0.15 μm pHEMT GaAs	3	Inductive	33 – 48	17 – 20	20	26 – 28	2 × 1.45
[10]	pHEMT GaAs	NA	NA	34 – 42	18.5	20 – 22	20 – 21	2.4 × 1.64
This work	0.1 μm pHEMT GaAs	3	Capacitive	32 – 40	18.5 – 25.5	30 – 35.5	19 – 20	2.3 × 1.5

30 ~ 35.5% with 19 ~ 20 dBm output power in 32 ~ 40 GHz.

A comparison of the Ka-band wideband PAs MMIC is shown in Table 1. The measured peak drain efficiency of final stage in our work is 46.3% at 36 GHz, which is higher than that of the single-stage PA^[2] (about 44.6% at 32GHz, calculated from its data). Most medium power amplifiers are designed for linear usage as^[8-9] with lower PAE about 20%. Hence, some high power amplifiers^[5-7] with high PAE are listed. Accounting the losses (approximately estimated to be 1% ~ 3% in PAE reducing) introduced by the power combining networks in high power amplifiers, the PAE (30% - 3% = 27%) of our work is still higher than the listed GaAs wideband PAs^[5-6] and comparable with GaN PA^[7].

Decided by the paralleling element closest to transistor, the output matching properties (capacitive /inductive) of these PAs are shown in this table. Their output matching performances can be roughly observed by S22. S22 of PA^[7-8] both present only one reflection zero for the bandwidth limitation of inductive matching. However, S22 of^[2] (lower operating band) and^[4] (narrower operating band) both achieve two reflection zeros with inductive matching, due to the limitation of i-matching only appearing at the high operating band wideband matching (shown as Eq. (13)). Because of its multi-section capacitive matching, S22 of PA^[5] presents five reflection zeros. Besides, S22 of our work has two reflection zeros (One is 33.5 GHz, the other is higher than 40 GHz.) with capacitive matching.

4 Conclusion

This paper presents a Ka-band high efficiency three-stage wideband PA MMIC with capacitive coupled matching structure. A set of formulas was proposed to calculate initial values of this matching and facilitate the optimization process. With the correcting of the frequency offset, these formulas are more accurate than those pres-

ented in Ref. [2]. The measured PAE of this PA is higher than 30% over the entire frequency band (32 ~ 40 GHz). These results demonstrate the effectiveness of this design method for millimeter wave wideband PA.

References

- [1] TANG Kan, FU Kun, SUN Xian, *et al.* Signature analysis and 3-D reconstruction of rectangular building in very high resolution SAR images [J]. *J. Infrared Millim. Waves* (唐侃, 付琨, 孙显等. 高分辨率 SAR 图像中矩形建筑物特性分析与三维重建. *红外与毫米波学报*), 2013, **32**(3): 198 – 204.
- [2] Huang P-C, Tsai Z-M, Lin K-Y, *et al.* A 17 – 35 GHz Broadband, High Efficiency PHEMT Power Amplifier Using Synthesized Transformer Matching Technique [J]. *IEEE Transactions on Microwave Theory and Techniques*, 2012, **60**(1): 112 – 119.
- [3] YANG Ge-Liang, WANG Zhi-Gong, LI Zhi-Qun, *et al.* Millimeter-wave Low Power UWB CMOS Common-gate LNA [J]. *J. Infrared Millim. Waves* (杨格亮, 王志功, 李智群等. CMOS 毫米波低功耗超宽带共栅低噪声放大器. *红外与毫米波学报*), 2014, **33**(6): 584 – 590.
- [4] Huang C W, Chang S J, Wu W, *et al.* Chang. A Three-Stage Ka Band PHEMT Wideband Amplifier MMIC [J]. *Microwave and Optical Technology Letters*, 2004, **42**(4): 277 – 280.
- [5] Campbell C F, Dumka D C, Kao M-Y, *et al.* Design and Performance of a High Efficiency Ka-band Power Amplifier MMIC [C]. 2010 IEEE Compound Semiconductor Integrated Circuit Symposium. Monterey, CA, 2010: 1 – 4.
- [6] TGA4516 Datasheet [R]. Oregon: TriQuint Semi, 2011.
- [7] Campbell C F, Liu Y, Kao M-Y, *et al.* High Efficiency Ka-Band Gallium Nitride Power Amplifier MMICs [C]. 2013 IEEE International Conference on Microwaves, Communications, Antennas and Electronics Systems. Tel Aviv, 2013: 1 – 5.
- [8] Chen S, Nayak S. A 1/2 Watt High Linearity and Wide Bandwidth PHEMT Driver Amplifier MMIC for Millimeter-Wave Applications [C]. IEEE MTT-S International Microwave Symposium Digest. San Francisco, CA, 2006: 1863 – 1866.
- [9] HMC-ABH264 Datasheet [R]. Massachusetts: Hittite Microwave Corp, 2015.
- [10] 0.1um GaAs PHEMT Device Model Handbook [R]. Taiwan: WIN Semiconductors Corp, 2013.

(上接 528 页)

- [16] Liu J, Xiao M, Shen J, *et al.* Flexible PMMA pipe for terahertz propagation [C]. *Photonics Asia. International Society for Optics and Photonics*, Beijing, 2012: 85620R – 85620R – 7.
- [17] Xiao M, Liu J, Zhang W, *et al.* THz wave transmission in thin-wall PMMA pipes fabricated by fiber drawing technique [J]. *Optics Communications*, 2013, **298**: 101 – 105.
- [18] Xiao M, Liu J, Zhang W, *et al.* Self-supporting polymer pipes for low loss single-mode THz transmission. [J]. *Optics Express*, 2013, **21**

(17): 19808 – 19815.

- [19] You B, Lu J Y, Yu C P, *et al.* Terahertz refractive index sensors using dielectric pipe waveguides [J]. *Optics Express*, 2012, **20**(6): 5858 – 66.
- [20] Centini M, Sibilina C, Scalora M, *et al.* Dispersive properties of finite, one-dimensional photonic band gap structures: applications to nonlinear quadratic interactions. [J]. *Physical Review E*, 1999, **60**(4): 4891.